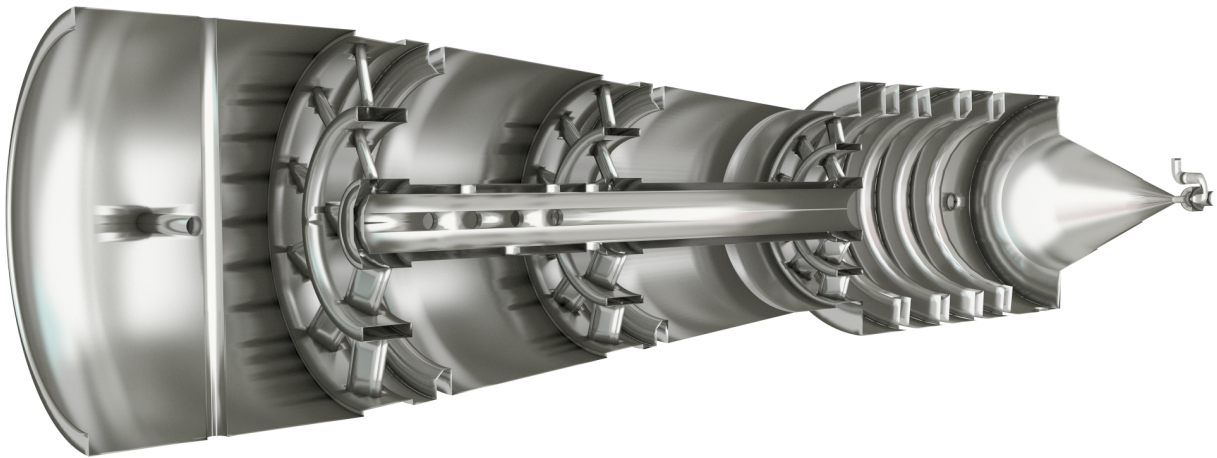


# NUMERICAL INVESTIGATION OF THE CFI BURNER



# Contents

	Page
<b>1 Introduction</b>	<b>1</b>
<b>2 Mathematical Basics</b>	<b>1</b>
2.1 Governing Equations . . . . .	1
2.2 Reynolds and Favre Averaging . . . . .	3
<b>3 Turbulence and Combustion Modeling</b>	<b>4</b>
3.1 Reynolds Stress Tensor and $k$ - $\omega$ SST Model . . . . .	4
3.2 Other Turbulent Fluxes . . . . .	5
3.3 Combustion Modeling . . . . .	6
3.4 Material Properties . . . . .	6
<b>4 Numerical Methods and Setup</b>	<b>7</b>
4.1 Element Based Finite Volume Method . . . . .	7
4.2 Computational Grid and Boundary Conditions . . . . .	8
4.3 Summary of the Numerical Setup . . . . .	11
<b>5 Simulation Results</b>	<b>12</b>
5.1 Flow Inside the Nozzles . . . . .	12
5.2 Flow Inside the Combustion Chamber . . . . .	12
5.3 Flow through the Pipe . . . . .	14
5.4 Setup A ( $\Phi \approx 3.4$ ) . . . . .	15
5.5 Setup B ( $\Phi = 1$ ) . . . . .	18
5.6 Setup C ( $\Phi \approx 0.83$ ) . . . . .	21
<b>6 Conclusion</b>	<b>24</b>
<b>7 Literature Recommendations</b>	<b>24</b>

# 1 INTRODUCTION

The simulation of the CFI burner was performed with the commercial software ANSYS CFX 5. This program implements the methods of Computational Fluid Dynamics (CFD) and has been used for a wide range of fluid-flow problems for over 20 years. To get a first impression of the burner's characteristics, methane was chosen as the fuel. This will be changed in future simulations.

The following section presents the mathematical basics to describe fluid motions and combustion processes. Section 3 shows how the turbulent fluctuations of the fluid and the chemical reactions are modeled in the CFX program, and what models were chosen for the simulation. In section 4, a quick overview over the numerical methods used to discretize and solve the system of differential equations is given, as well as an overview of the computational grid. Section 5 presents the results of selected simulations of the burner for different modes of operation. In the last section improvements for the burner are proposed based on the simulation results.

## 2 MATHEMATICAL BASICS

The motion of a fluid is described by the governing equations of fluid dynamics. These equations represent the conservation of total mass and momentum (*Navier-Stokes equations*). In the case of a reacting mixture, the conservation of energy and species masses have to be considered as well. These equations form a system of partial, non-linear and coupled differential equations that have to be solved numerically.

### 2.1 GOVERNING EQUATIONS

The conservation equations can be expressed in the form of balance or transport equations:

$$\underbrace{\frac{\partial(\rho\phi)}{\partial t}}_{\textcircled{1}} + \underbrace{\nabla \cdot (\rho u \phi)}_{\textcircled{2}} = \underbrace{-\nabla \cdot j_\phi}_{\textcircled{3}} + S_\phi \quad (1)$$

This equation describes the transport of an arbitrary quantity  $\phi$ .  $\rho$  is the mixture density,  $t$  the time and  $u$  the fluid velocity. Term  $\textcircled{1}$  is the accumulation of  $\phi$  over time.  $\textcircled{2}$  is the advection of the quantity  $\phi$  with the fluid flow. Term  $\textcircled{3}$  is the diffusion of  $\phi$ . It is usually written as

$$j_\phi = -\Gamma \nabla \phi \quad (2)$$

with  $\Gamma$  being the corresponding diffusion coefficient.  $S_\phi$  is a source term for  $\phi$  and summarizes all processes that do not fit into the previous three terms.

By setting  $\phi = 1$  in Eq. (1) and omitting any source terms, the conservation of total mass is obtained. This can be derived by balancing the net mass fluxes through the surfaces of an Eulerian control volume. For a compressible fluid in its conservative form the conservation of total mass can be expressed as:

$$\frac{\partial \rho}{\partial t} + \nabla \cdot (\rho u) = 0 \quad (3)$$

The conservation of momentum can be formulated as the transport of the velocity  $u$  (setting  $\phi = u$  in Eq. (1)). This can be derived by balancing the forces acting on the fluid inside a control volume.

$$\frac{\partial(\rho u)}{\partial t} + \nabla \cdot (\rho u u) = -\nabla p + \nabla \cdot \tau + \rho g \quad (4)$$

$p$  is the pressure and  $uu$  the dyadic product of two velocity vectors.  $g$  is the standard gravitational acceleration, which is neglected in this simulation due to the generally high velocities. The

molecular or laminar stress tensor  $\tau$  is needed to describe the diffusive momentum flux. For a compressible Newtonian fluid it can be obtained by using the Stokes assumption:

$$\tau = \mu \left( \nabla u + (\nabla u)^T - \frac{2}{3} I \nabla \cdot u \right) \quad (5)$$

$\mu$  is the dynamic viscosity and  $I$  the identity matrix.

The conservation of species mass is expressed by the transport of the mass fraction  $Y_i$  of species  $i$  ( $\phi = Y_i$ ), and assuming Fick's law for the diffusion term:

$$\frac{\partial(\rho Y_i)}{\partial t} + \nabla \cdot (\rho u Y_i) = \nabla \cdot (\Gamma_i \nabla Y_i) + M_i R_i \quad (6)$$

$\Gamma_i$  is the mass diffusion coefficient of species  $i$ ,  $M_i$  its molecular weight and  $R_i$  its reaction rate. In the given scenario the species  $i$  can represent either  $O_2$ ,  $N_2$ ,  $CH_4$ ,  $H_2O$  or  $CO_2$ .  $Y_i$  is defined as:

$$Y_i = \frac{m_i}{\sum_{j=1}^N m_j} \quad (7)$$

$m_i$  is the mass of species  $i$  and  $N$  the number of species. For  $N_2$  no transport equation is solved, because the species mass transport equations form an overdetermined system with the total mass conservation.

The conservation of energy can be derived by balancing the total energy (internal energy  $e$  and kinetic energy), including the energy flux due to mass diffusion, and using the relation:

$$e = h - \frac{p}{\rho} \quad (8)$$

$h$  is the mixture enthalpy. The transport equation for the total energy  $h_{tot}$

$$h_{tot} = h + \frac{1}{2} u \cdot u \quad (9)$$

can be written as:

$$\frac{\partial(\rho h_{tot})}{\partial t} + \nabla \cdot (\rho u h_{tot}) = \nabla \cdot (\lambda \nabla T) + \nabla \cdot \left( \sum_{i=1}^N h_i \Gamma_i \nabla Y_i \right) + \frac{\partial p}{\partial t} + \nabla \cdot (\tau \cdot u) \quad (10)$$

$h_i$  is the enthalpy of the species  $i$ ,  $\lambda$  the thermal conductivity of the mixture and  $T$  the temperature. The viscous work term  $\nabla \cdot (\tau \cdot u)$ , as well as heat transfer due to radiation are neglected in this simulation.

In summary, the system of differential equations consists of one transport equation for the total mass, three momentum conservation equations (for all three spatial dimensions),  $N - 1$  species mass conservation equations and one energy conservation equation. To close this system, equations of state for the density and mixture enthalpy, that connect both quantities to pressure and temperature, have to be defined. Because the fluid in this simulation is assumed to be an ideal gas, the relation between density and pressure is given by the ideal gas law:

$$\rho = \frac{p}{R_s T} \quad (11)$$

$R_s$  is the specific gas constant of the mixture. For an ideal gas the relation between enthalpy and temperature can be reduced to:

$$dh = c_p dT \quad (12)$$

$c_p$  is the specific isobaric heat capacity of the mixture.

## 2.2 REYNOLDS AND FAVRE AVERAGING

Directly solving the governing equations as presented in the previous section is too computationally expensive, because it would require to resolve all relevant time and length scales. Instead, the RANS (*Reynolds Averaged Navier-Stokes equations*) method is used. Hereby, the governing equations are averaged over time. The general idea is to only resolve the time averaged mean flow. The turbulent fluctuations can then be modeled separately.

For example, the time averaging for the generic quantity  $\phi$  can be written as:

$$\bar{\phi} = \frac{1}{\Delta t} \int_{t_0}^{t_0+\Delta t} \phi dt \quad (13)$$

The instantaneous value  $\phi$  can be split into the averaged mean value  $\bar{\phi}$  and a fluctuation  $\phi'$  around the average:

$$\phi = \bar{\phi} + \phi' \quad (14)$$

By using the averaging rules

$$\overline{a+b} = \bar{a} + \bar{b}, \quad \overline{\nabla a} = \nabla \bar{a}, \quad \bar{\bar{a}} = \bar{a}, \quad \bar{a'} = 0 \quad (15)$$

and simplifying the diffusive term to  $\nabla \cdot j_\phi$  for now, the averaged generic transport equation is given by:

$$\overline{\frac{\partial(\rho\phi)}{\partial t} + \nabla \cdot (\rho u\phi)} = \overline{\nabla \cdot j_\phi + S_\phi} \rightarrow \frac{\partial(\bar{\rho}\bar{\phi})}{\partial t} + \nabla \cdot (\bar{\rho}u\bar{\phi}) = \nabla \cdot \bar{j}_\phi + \bar{S}_\phi \quad (16)$$

Because the change in density cannot be neglected for combustion processes, the correlation terms  $\bar{\rho\phi}$  and  $\overline{\rho u\phi}$  have to be expressed in a different form. By introducing a density weighted average (*Favre averaging*) these terms can be simplified. The density weighted average is defined as:

$$\tilde{\phi} = \frac{\frac{1}{\Delta t} \int_{t_0}^{t_0+\Delta t} \rho\phi dt}{\frac{1}{\Delta t} \int_{t_0}^{t_0+\Delta t} \rho dt} = \frac{\overline{\rho\phi}}{\bar{\rho}} \quad (17)$$

Again, the quantity  $\phi$  can be split into the density weighted mean  $\tilde{\phi}$  and a turbulent fluctuation  $\phi''$ :

$$\phi = \tilde{\phi} + \phi'' \quad (18)$$

By using the Favre averaging method, substituting Eq. (18) and applying the averaging rules

$$\widetilde{\tilde{\phi}''} = 0, \quad \tilde{\tilde{\phi}} = \tilde{\phi}, \quad \widetilde{\tilde{\phi}\phi''} = 0 \quad (19)$$

the correlation terms can now be rewritten to:

$$\overline{\rho\phi} = \bar{\rho}\tilde{\phi} \quad (20)$$

$$\overline{\rho u\phi} = \bar{\rho}\widetilde{u\phi} = \bar{\rho}\tilde{u}\tilde{\phi} + \bar{\rho}\widetilde{u''\phi''} \quad (21)$$

Introducing an approximation for the averaged diffusion term

$$\bar{j}_\phi = \bar{\Gamma}\bar{\nabla}\bar{\phi} \approx \Gamma\nabla\tilde{\phi} \quad (22)$$

the Favre averaged transport equation becomes:

$$\frac{\partial(\bar{\rho}\tilde{\phi})}{\partial t} + \nabla \cdot (\bar{\rho}\tilde{u}\tilde{\phi}) = \Gamma\nabla\tilde{\phi} - \nabla \cdot (\bar{\rho}\widetilde{u''\phi''}) + \bar{S}_\phi \quad (23)$$

This equation has the same form as the original equation except for the additional term on the right hand side containing the turbulent fluctuations. Because the governing equations are

solved with regards to the averaged variables, the turbulent fluctuations are unknown. So in order to close the system of differential equations they have to be modeled (see the next section).

Applying this methodology to the conservation equations, the Favre averaged transport equations are obtained:

$$\frac{\partial \bar{\rho}}{\partial t} + \nabla \cdot (\bar{\rho} \tilde{u}) = 0 \quad (24)$$

$$\frac{\partial (\bar{\rho} \tilde{u})}{\partial t} + \nabla \cdot (\bar{\rho} \tilde{u} \tilde{u}) = -\nabla \bar{p} + \nabla \cdot \bar{\tau} - \nabla \cdot (\bar{\rho} \widetilde{u'' u''}) \quad (25)$$

$$\frac{\partial (\bar{\rho} \tilde{Y}_i)}{\partial t} + \nabla \cdot (\bar{\rho} \tilde{u} \tilde{Y}_i) = \nabla \cdot (\Gamma_i \nabla \tilde{Y}_i) - \nabla \cdot (\bar{\rho} \widetilde{u'' Y_i''}) + M_i \bar{R}_i \quad (26)$$

$$\frac{\partial (\bar{\rho} \tilde{h}_{tot})}{\partial t} + \nabla \cdot (\bar{\rho} \tilde{u} \tilde{h}_{tot}) = \frac{\partial \bar{p}}{\partial t} + \nabla \cdot \left( \lambda \nabla \tilde{T} + \sum_{i=1}^N h_i \Gamma_i \nabla \tilde{Y}_i \right) - \nabla \cdot (\bar{\rho} \widetilde{u'' h''}) \quad (27)$$

### 3 TURBULENCE AND COMBUSTION MODELING

As seen in the previous section, the turbulent fluctuations in the averaged governing equations are unknown. Eq. (23) shows that these correlation terms have the same form as the laminar diffusive terms. This can be summarized by combining both terms into the diffusive term:

$$\frac{\partial (\bar{\rho} \tilde{\phi})}{\partial t} + \nabla \cdot (\bar{\rho} \tilde{u} \tilde{\phi}) = \nabla \cdot (\Gamma \nabla \tilde{\phi} - \bar{\rho} \widetilde{u'' \phi''}) + \bar{S}_\phi \quad (28)$$

Because the turbulent fluxes act the same way as the molecular diffusion, a gradient assumption analogous to the molecular diffusion term is used to model the turbulent correlation terms:

$$-\bar{\rho} \widetilde{u'' \phi''} \approx \Gamma_t \nabla \tilde{\phi} \quad (29)$$

Now the fluxes can be expressed with the mean quantity gradient  $\nabla \tilde{\phi}$ . The only unknown variable is the turbulent diffusion coefficient  $\Gamma_t$ . Its closure will be discussed later on. The generic transport equation now simplifies to:

$$\frac{\partial (\bar{\rho} \tilde{\phi})}{\partial t} + \nabla \cdot (\bar{\rho} \tilde{u} \tilde{\phi}) = \nabla \cdot ((\Gamma + \Gamma_t) \nabla \tilde{\phi}) + \bar{S}_\phi \quad (30)$$

#### 3.1 REYNOLDS STRESS TENSOR AND $k$ - $\omega$ SST MODEL

The turbulent correlation term in the momentum equation is called *Reynolds Stress Tensor*, because it acts the same way as the laminar stress tensor. By using the gradient assumption analogously to the molecular stress tensor, the Reynolds Stress Tensor can be written as:

$$-\bar{\rho} \widetilde{u'' u''} \approx \mu_t \left( \nabla \tilde{u} + (\nabla \tilde{u})^T - \frac{2}{3} I \nabla \cdot \tilde{u} \right) - \frac{2}{3} I \bar{\rho} \tilde{k} \equiv \tilde{\tau}_t \quad (31)$$

$\tilde{k}$  is the turbulent kinetic energy:

$$\tilde{k} \equiv \frac{1}{2} \widetilde{u'' \cdot u''} \quad (32)$$

Now, the only unknown variables in this equation are the turbulent kinetic energy  $\tilde{k}$  and the turbulent “viscosity”  $\mu_t$ .

The turbulence model used in this simulation is the  $k$ - $\omega$  SST (*Shear Stress Transport*) model. It assumes that the turbulent viscosity (*eddy viscosity*) can be expressed as follows:

$$\mu_t = \frac{\bar{\rho} c_1 \tilde{k}}{\max(c_1 \tilde{\omega}, F)} \quad (33)$$

$\omega$  is the specific rate of the turbulent kinetic energy dissipation,  $c_1$  is a model constant and  $F$  is a blending function that corrects the turbulent fluxes depending on the flow field and wall distance (for further information see the CFX documentation). The  $k$ - $\omega$  model is a two-equation model. Therefore, two additional transport equations are solved for  $\tilde{k}$  and  $\tilde{\omega}$ :

$$\frac{\partial(\bar{\rho}\tilde{k})}{\partial t} + \nabla \cdot (\bar{\rho}\tilde{u}\tilde{k}) = \nabla \cdot \left( \left( \mu + \frac{\mu_t}{\sigma_1} \right) \nabla \tilde{k} \right) + \tilde{\tau}_t : \nabla \tilde{u} - \sigma_2 \bar{\rho} \tilde{k} \tilde{\omega} + S_k \quad (34)$$

$$\frac{\partial(\bar{\rho}\tilde{\omega})}{\partial t} + \nabla \cdot (\bar{\rho}\tilde{u}\tilde{\omega}) = \nabla \cdot \left( \left( \mu + \frac{\mu_t}{\sigma_3} \right) \nabla \tilde{\omega} \right) + S_\omega \quad (35)$$

$\sigma_1$ ,  $\sigma_2$  and  $\sigma_3$  are model constants.  $S_\omega$  and  $S_k$  are source terms containing several blending and limiter functions (see the CFX documentation for the specific implementation). With these two additional transport equations, no further unknown variables remain and the Reynolds Stress Tensor can be computed. With the final assumption

$$\bar{\tau} = \overline{\tilde{\tau} + \tau''} \approx \tilde{\tau} \quad (36)$$

the momentum conservation equation becomes:

$$\frac{\partial(\bar{\rho}\tilde{u})}{\partial t} + \nabla \cdot (\bar{\rho}\tilde{u}\tilde{u}) = -\nabla \bar{p} + \nabla \cdot \left( (\mu + \mu_t) \left( \nabla \tilde{u} + (\nabla \tilde{u})^T - \frac{2}{3} I \nabla \cdot \tilde{u} \right) - \frac{2}{3} I \bar{\rho} \tilde{k} \right) \quad (37)$$

In CFX the velocity divergence term  $\frac{2}{3} I \nabla \cdot \tilde{u}$  is neglected.

## 3.2 OTHER TURBULENT FLUXES

The turbulent flux of species mass is also assumed to follow the gradient assumption:

$$-\bar{\rho} \widetilde{u''Y_i''} \approx \frac{\mu_t}{Sc_t} \nabla \tilde{Y}_i \quad (38)$$

In this simulation,  $Sc_t$  is assumed to be 0.9. The conservation of species mass simplifies to:

$$\frac{\partial(\bar{\rho}\tilde{Y}_i)}{\partial t} + \nabla \cdot (\bar{\rho}\tilde{u}\tilde{Y}_i) = \nabla \cdot \left( \left( \Gamma_i + \frac{\mu_t}{Sc_t} \right) \nabla \tilde{Y}_i \right) + M_i \bar{R}_i \quad (39)$$

The derivation of the energy transport equation is a bit more laborious, so only the final result for an ideal gas mixture with  $Pr_t = Sc_t = 0.9$  is presented here (for the full derivation see the CFX documentation):

$$\frac{\partial(\bar{\rho}\tilde{h}_{tot})}{\partial t} + \nabla \cdot (\bar{\rho}\tilde{u}\tilde{h}_{tot}) = \frac{\partial \bar{p}}{\partial t} + \nabla \cdot \left( \left( \lambda + c_p \frac{\mu_t}{Pr_t} \right) \nabla \tilde{T} + \sum_{i=1}^N \tilde{h}_i \left( \Gamma_i + \frac{\mu_t}{Sc_t} \right) \nabla \tilde{Y}_i \right) \quad (40)$$

with

$$\tilde{h}_{tot} = \tilde{h} + \frac{1}{2} \tilde{u} \cdot \tilde{u} + \tilde{k} \quad (41)$$

### 3.3 COMBUSTION MODELING

The reaction rates, which appear as a source term in the species mass transport equations, are calculated by using a *Finite Rate Chemistry* approach. In this simulation a global, irreversible single-step reaction is used:



The reaction rate of this reaction is then computed by assuming an Arrhenius temperature dependence:

$$\bar{R}_i = \nu_i \cdot 8.3 \cdot 10^6 \frac{1}{\text{s}} \exp\left(-\frac{30 \frac{\text{kcal}}{\text{mol}}}{\mathcal{R}\tilde{T}}\right) C_{\text{CH}_4}^{-0.3} C_{\text{O}_2}^{1.3} \quad (43)$$

$\mathcal{R}$  is the universal gas constant,  $\nu_i$  is the stoichiometric coefficient of species  $i$  in the single-step reaction and  $C_{\text{CH}_4}$  and  $C_{\text{O}_2}$  are the concentrations of methane and oxygen. Additionally, the reaction rates are limited to keep the species mass fractions between zero and one:

$$\bar{R}_{Prod} \equiv \bar{R}_{Prod} \cdot \frac{1 - \tilde{Y}_{Prod}}{\max(10^{-6}, 1 - \tilde{Y}_{Prod})}, \quad \bar{R}_{React} \equiv \bar{R}_{React} \cdot \frac{\tilde{Y}_{React}}{\max(10^{-6}, \tilde{Y}_{React})} \quad (44)$$

As the product mass fractions approach one or the reactant mass fractions approach zero, their respective reaction rates are forced to zero.

Because the reaction rates have a strong temperature dependence, the resulting system of differential equations tends to be very stiff. Thus, special algorithms have to be selected to solve these equations.

### 3.4 MATERIAL PROPERTIES

Lastly, the material properties are computed as follows: The species viscosities  $\mu_i$  and heat conductivities  $\lambda_i$  are assumed to be constant and are taken from the CFX material database. The species mass diffusion coefficients  $\Gamma_i$  are assumed to be equal to  $\mu_i$  ( $\text{Sc}_i = 1$ ). The heat capacities and species enthalpies are calculated from NASA-polynomials:

$$\tilde{h}_i = \frac{\mathcal{R}}{M_i} \left( a_{i,6} + a_{i,1}\tilde{T} + \frac{a_{i,2}}{2}\tilde{T}^2 + \frac{a_{i,3}}{3}\tilde{T}^3 + \frac{a_{i,4}}{4}\tilde{T}^4 + \frac{a_{i,5}}{5}\tilde{T}^5 \right) \quad (45)$$

$$c_{p,i} = \frac{\mathcal{R}}{M_i} \left( a_{i,1} + a_{i,2}\tilde{T} + a_{i,3}\tilde{T}^2 + a_{i,4}\tilde{T}^3 + a_{i,5}\tilde{T}^4 \right) \quad (46)$$

The coefficients  $a_{i,j}$  are taken from the CFX database too. Additionally, for every species two sets of coefficients are used - one set for temperatures up to 1000 K and one above 1000 K. All mixture properties are assumed to be mass weighted:

$$\alpha = \sum_{i=1}^N \tilde{Y}_i \alpha_i \quad (47)$$

$\alpha$  can be the enthalpy  $\tilde{h}$ , heat capacity  $c_p$ , viscosity  $\mu$  or heat conductivity  $\lambda$ . The Favre averaged equation of state for the density is approximated by:

$$\bar{\rho} \approx \frac{\bar{p}}{\tilde{T}\mathcal{R} \sum_{i=1}^N \frac{\tilde{Y}_i}{M_i}} \quad (48)$$

The temperature is calculated from the mixture enthalpy by using the Newton-Raphson method:

$$\tilde{T}_{n+1} = \tilde{T}_n + \frac{\tilde{h}_n - \tilde{h}_0}{c_{p,n}} \quad (49)$$

## 4 NUMERICAL METHODS AND SETUP

The system of governing equations cannot be solved analytically. In order to solve it numerically, the differential equations first have to be transformed into algebraic equations. This is done by applying a discretization method, whereby the solutions are approximated only at discrete points in space (and time). Therefore, a computational grid (*mesh*) has to be provided that defines the positions of these discrete points. The discretization method used by CFX is a *Finite Volume Method* based on the *Finite Element Method* called *Element Based Finite Volume Method*.

### 4.1 ELEMENT BASED FINITE VOLUME METHOD

The main idea of the Finite Volume Method is to split up the computational domain into control volumes and solve the conservation equations for these volumes. Therefore, the computational grid is made up of nodes (Figure 1). Each node is the center of a control volume. Additionally, the discrete solution values are only saved at the node positions. The nodes span elements that provide shape functions to interpolate the discrete solution values at arbitrary positions. The elements are also split up into sectors, which are used to calculate volume integrals.

The following section shows this procedure for the generic transport equation (Eq. (1)). The methodology described here can be applied to all mentioned Favre averaged governing equations in the same way. Integrating the stationary transport equation over a control volume, and using the Gauss divergence theorem leads to:

$$\int_S \rho u \phi dA = \int_S \Gamma \nabla \phi dA + \int_V S_\phi dV \quad (50)$$

$A$  is the surface area of the control volume and  $V$  its volume. To discretize this equation, values at the *interpolation points* (*ip*) are assumed to be representative for their section of the control volume surface. The surface integrals can then be reduced to a sum over the surface sections. The volume integral is solved for each element sector by averaging the values at the sector

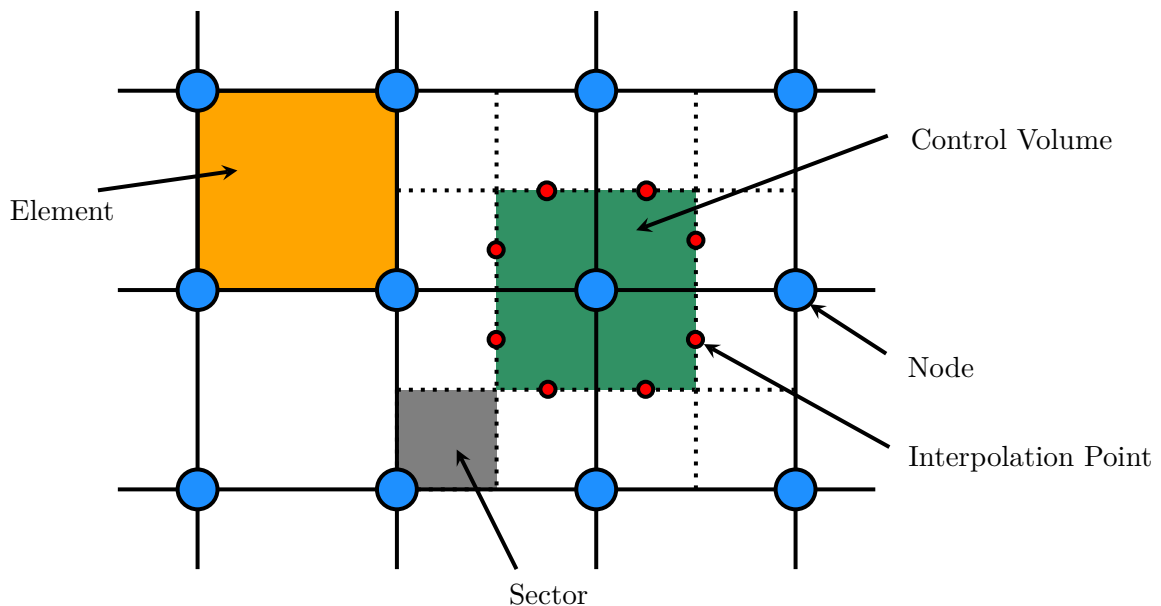


**Figure 1:** Simplified view of the different volumes in the computational grid. Every node (blue) is the center of a control volume (green). The nodes itself span elements (orange) which are subdivided into sectors (gray).

vertices (see Eq. (52)) and then summing them up for the control volume.

$$\sum_{ip} (\rho u \phi)_{ip} A_{ip} = \sum_{ip} (\Gamma \nabla \phi)_{ip} A_{ip} + S_\phi V \quad (51)$$

$ip$  is the center-point of the surface section with area  $A_{ip}$ . Because the values at the interpolation points are not known, shape functions are used to interpolate the solution values from the node positions to arbitrary positions  $x$ :

$$\phi_x = \sum_n \phi_n N_n(x) \quad (52)$$

$\phi_n$  are the known solution values at the nodes.  $N_n(x)$  is a tri-linear shape function of node  $n$  at the position  $x$ . It depends on the form of the element containing the position  $x$ .

In this simulation, the advection term is discretized by the second order central difference scheme. Using Eq. (52) to interpolate the values at position  $ip$  from the known nodal values, the advection term becomes:

$$\int_S \rho u \phi dA \approx \sum_{ip} (\rho u \phi)_{ip} A_{ip} = \sum_{ip} \left( A_{ip} \sum_n (\rho u \phi)_n N_n(ip) \right) \quad (53)$$

The diffusion term discretization follows the Finite Element Method too. Using the discretization of the local gradient

$$\nabla \phi_x = \sum_n \phi_n \nabla N_n(x) \quad (54)$$

the diffusion term can be written as:

$$\int_S \Gamma \nabla \phi dA \approx \sum_{ip} (\Gamma \nabla \phi)_{ip} A_{ip} = \sum_{ip} \left( A_{ip} \Gamma_{ip} \sum_n \phi_n \nabla N_n(ip) \right) \quad (55)$$

$\Gamma_{ip}$  can be interpolated following Eq. (52). Now, all terms in Eq. (50) only depend on values at the node locations. Because of this, a system of linearized equations can be created. After substituting Eq. (53) and Eq. (55) into Eq. (50) and factoring out the values  $\phi_n$  from the discretized governing equations, a linearized equation for each control volume with the center node  $k$  is obtained:

$$a_k \phi_k + \sum_n a_n \phi_n = b_k \quad (56)$$

$n$  are the nodes adjacent to the center node  $k$  and  $a_n$  are the factored out parts of the discretized equations.  $b_k$  is the source term for the control volume  $k$ .

The system of linear equations (one equation per node and transport equation) is then solved iteratively by an Algebraic Multigrid accelerated Incomplete Lower Upper solver. First, the momentum equations and the total mass conservation equation are coupled and solved together. A special velocity-pressure coupling is applied to account for the co-located storage of pressure and velocity values, as well as to predict the mass fluxes in an implicit way (see the CFX documentation for details). Then, the energy equation is solved. Lastly, the species mass conservation equations are solved as a coupled system as well. After all governing equations have been solved in this manner, another system of linearized equations with the new values of  $\phi$  is created and the next iteration begins.

## 4.2 COMPUTATIONAL GRID AND BOUNDARY CONDITIONS

The computational grid used for this simulation consists of about three million nodes and 16 million elements, most of which have a tetrahedral shape. A full run on this grid takes about 200 CPU hours. The simulations were performed on the computing cluster of the Division of

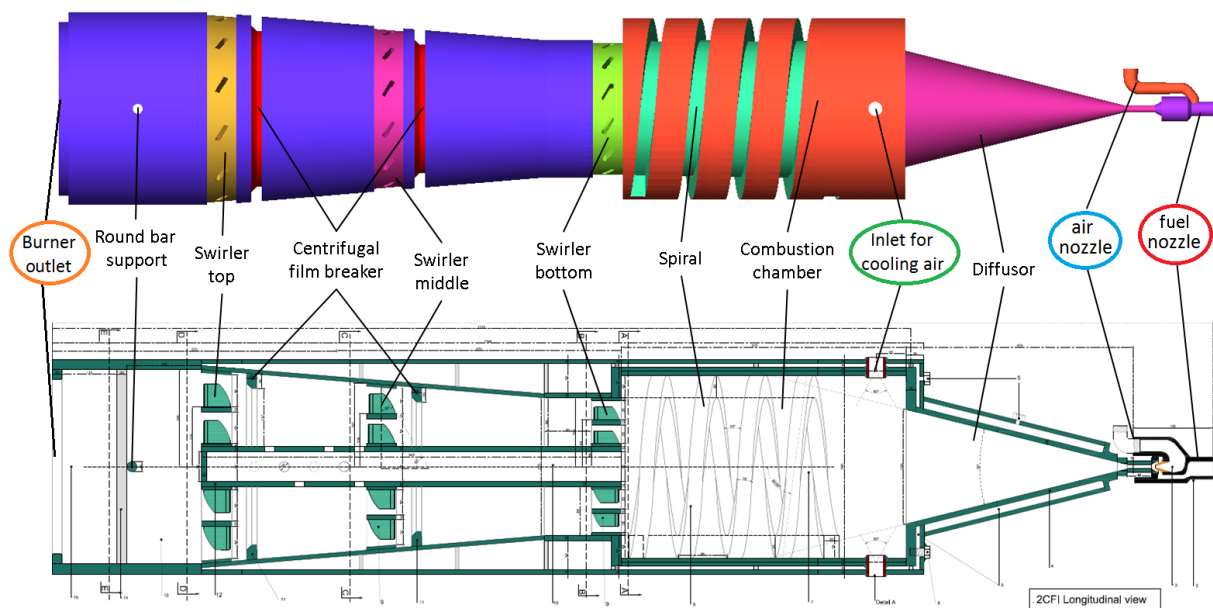


**Figure 2:** Longitudinal view of the burner geometry. There are three types of inlets into the burner that will be referenced in the following sections: the fuel nozzle (red circle), the air nozzle (blue circle) and the inlets for the cooling air (green circle). The Reynolds number of the burner used in the description of the numerical setup is based on the burner outlet (orange circle)

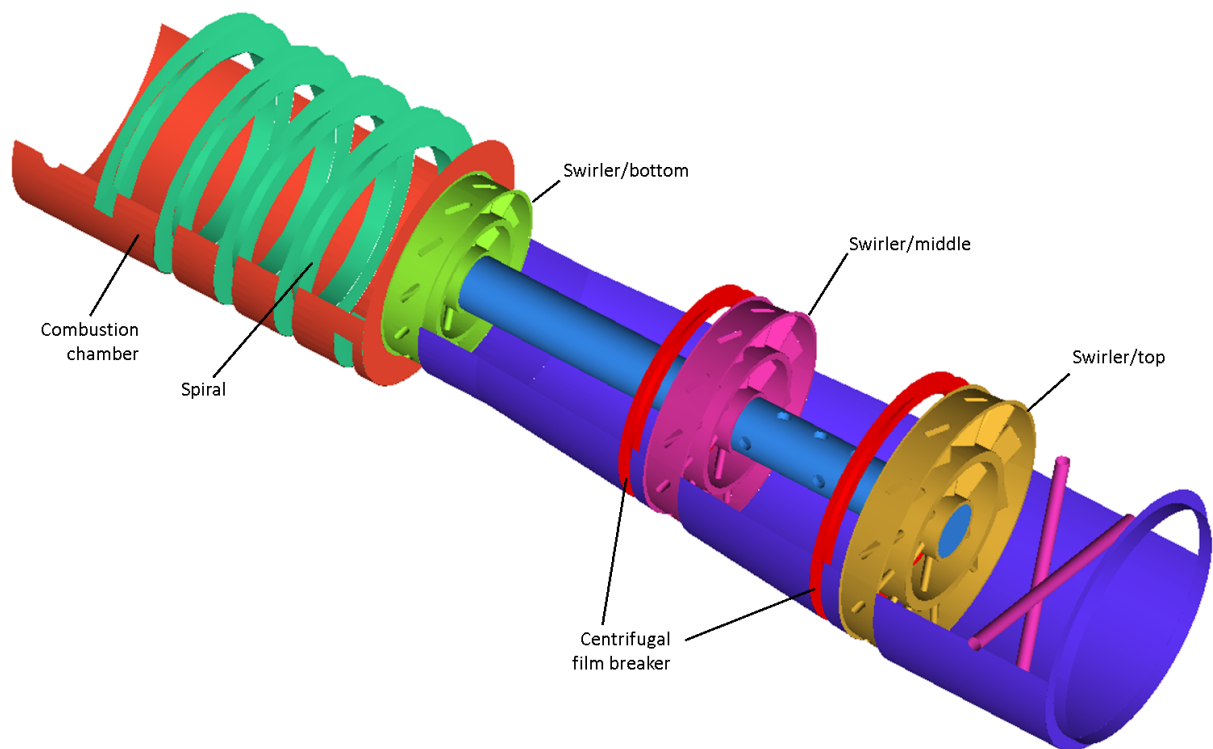


**Figure 3:** View inside the burner geometry.

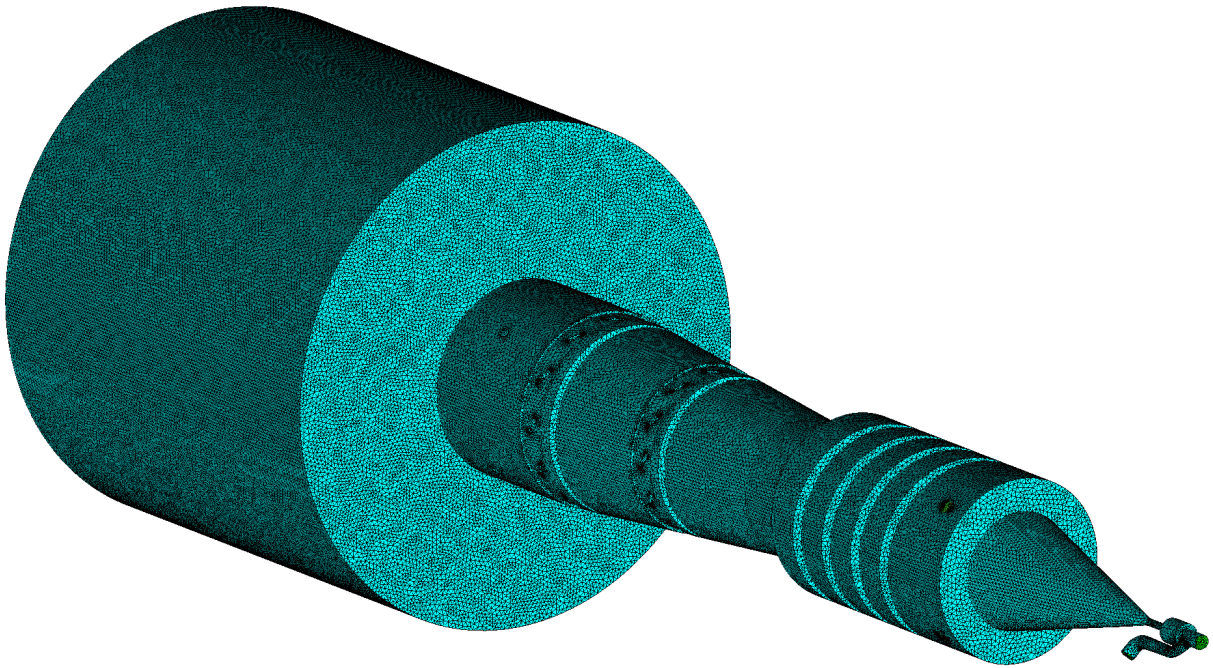


**Figure 4:** *Complete computational grid, including the cylindrical shaped burner environment at the burner outlet.*

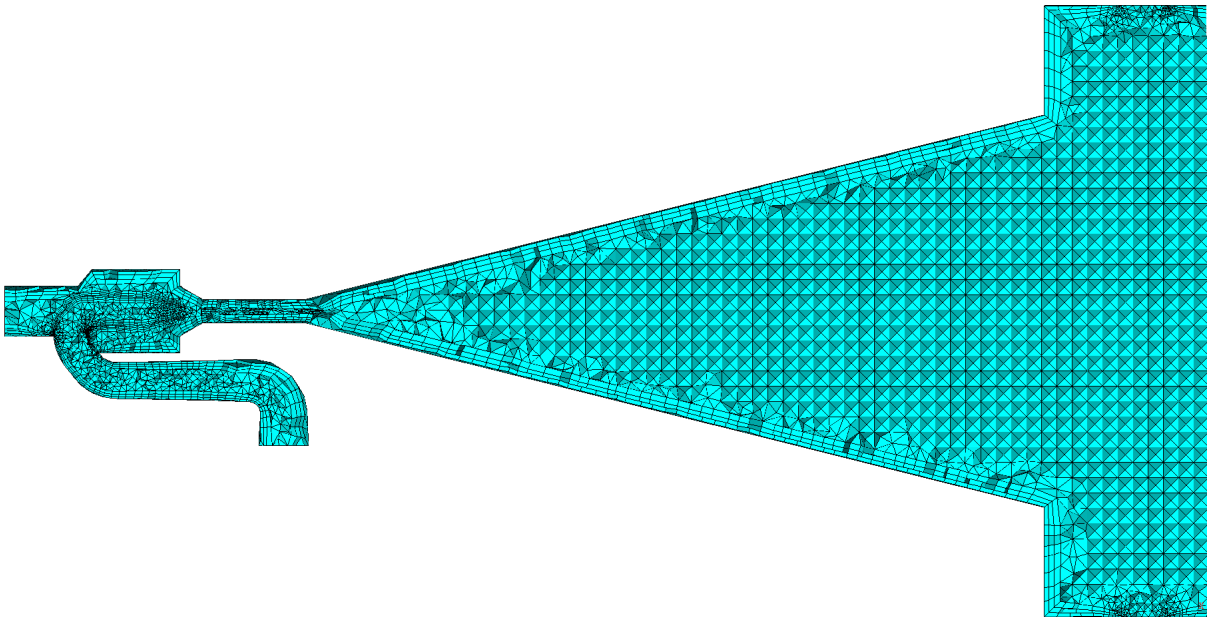


**Figure 5:** *Magnified view of the mesh inside the nozzles and the diffuser. The computational domain consists mostly of tetrahedral shaped elements.*

Combustion Technology at the Engler-Bunte-Institute. To execute the simulation in parallel, the computational domain is decomposed into smaller sections and distributed onto the CPUs of the cluster.

Because the Navier-Stokes equations are boundary value problems, the boundary conditions of the computational domain have to be specified. The domain is bounded by three types of regions:

- *inlet* regions are the entry point of fluid into the domain.
- *openings* define the environment conditions and are mostly exit points for mass flows.
- the solid surfaces of the burner are *walls*.

In this simulation, there are three types of inlets: The inlet into the air nozzle, the inlet into the fuel nozzle and four inlets for the cooling air into the combustion chamber (see Figure 2). All fluids entering the domain via the inlets or the opening, as well as the burner environment have a temperature of 300 K. The burner walls are assumed to be adiabatic. This is done by enforcing the temperature gradient in the direction of the walls to be zero. The pressure of the burner environment is 1 atm.

At the inlets, the fluid mass flow rates are set. The fluid velocities  $U$  are then calculated by

$$U_{inlet} = \frac{\dot{m}_{inlet}}{\bar{\rho}A} \quad (57)$$

$A$  is the inlet area and  $\dot{m}$  the mass flow rate. The velocity direction is the surface normal of the inlet. At the walls, the velocity is set to zero to ensure the no-slip condition.

The air is assumed to be composed of  $Y_{O_2} = 0.233$  and  $Y_{N_2} = 0.767$ . At the inlets, the mass fractions are fixed - the air nozzle inlet, the cooling air inlets and the burner environment have the air composition, whereas the fuel nozzle inlet has a fixed value of  $Y_{CH_4} = 1$ .

As a first guess, the turbulent intensity  $I$  at all inlets is set to 5 %. This can be adjusted in future simulations. The turbulent kinetic energy  $\tilde{k}$  and  $\tilde{\omega}$  are calculated by:

$$\tilde{k}_{inlet} = \frac{3}{2}I^2U_{inlet}^2 \quad (58)$$

$$\tilde{\omega}_{inlet} = \bar{\rho}(1000 \cdot I\mu)^{-1} \quad (59)$$

The flow near the walls is additionally modeled by wall functions: Because the computational grid cannot fully resolve the viscous sublayer, empirical formulations are used to describe the transport processes in wall near regions. The method used by CFX blends between scalable wall functions and  $\omega$ -based models (for details, see the CFX documentation).

### 4.3 SUMMARY OF THE NUMERICAL SETUP

To obtain adequate initial values for the simulation, some preceding simulations have been performed:

- The first step is a simulation on a coarse grid using first order discretizations with the *Eddy Breakup Model*. This is done to ignite the gas in the combustion chamber.
- Then, still using the coarse grid and first order discretizations, an approximate solution with the *Finite Rate Chemistry* approach is created.

The last results are then used as initial values for the finer grid and the setup summarized below:

- the final simulation is done using the stationary 3D RANS method and the SST  $k-\omega$  turbulence model.

- a second order discretization scheme for the advection terms is applied.
- combustion is modeled by the Finite Rate Chemistry approach using a single-step reaction for methane as fuel.
- the computational grid consists of three million nodes. Because of this, each simulation takes about 200 CPU hours.
- the fluid is a compressible and ideal gas, as well as an ideal mixture.

## 5 SIMULATION RESULTS

One constraint of the simulation is to stay below the speed of sound at the air nozzle outlet (see Figure 2). This limits the air flow rate to about 0.01 kg/s. For the different simulation setups described later in this section, the fuel flow rates have been varied. The corresponding air-fuel equivalence ratios  $\Phi$  are given in the setup summaries. The cooling air flow rate is set to 0.08 kg/s, resulting in a Reynolds number of  $Re \approx 3 \cdot 10^4$  at the burner outlet (Figure 2).

### 5.1 FLOW INSIDE THE NOZZLES

Because the fuel cannot flow around the air nozzle symmetrically, a back flow below and to the sides of the air nozzle arises. Depending on the ratio of fuel to air mass flow rates, this recirculation zone contains an ignitable mixture (see Figure 6).

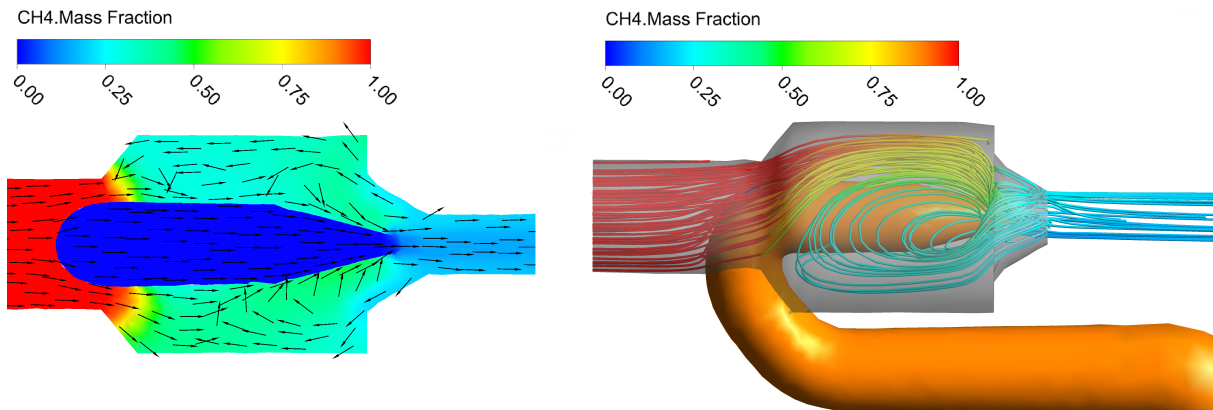


**Figure 6:** Fuel flow around the air nozzle for setup A. Left: cross section. Right: 3D side view.

### 5.2 FLOW INSIDE THE COMBUSTION CHAMBER

The spiral inside the combustion chamber does not generate any swirl for the fluid flow. Instead, the spiral's edges create recirculation zones. Additionally, a strong back flow at the end of the diffuser arises. This is illustrated in Figure 7 and Figure 8. Another consequence of the unsymmetrical flow field inside the nozzle is that the fuel/air mixture flow is directed upwards in the diffuser. This can be seen in Figure 8 and is most noticeable in the stream line pictures of setup B and setup C (Figures 15 and 18).

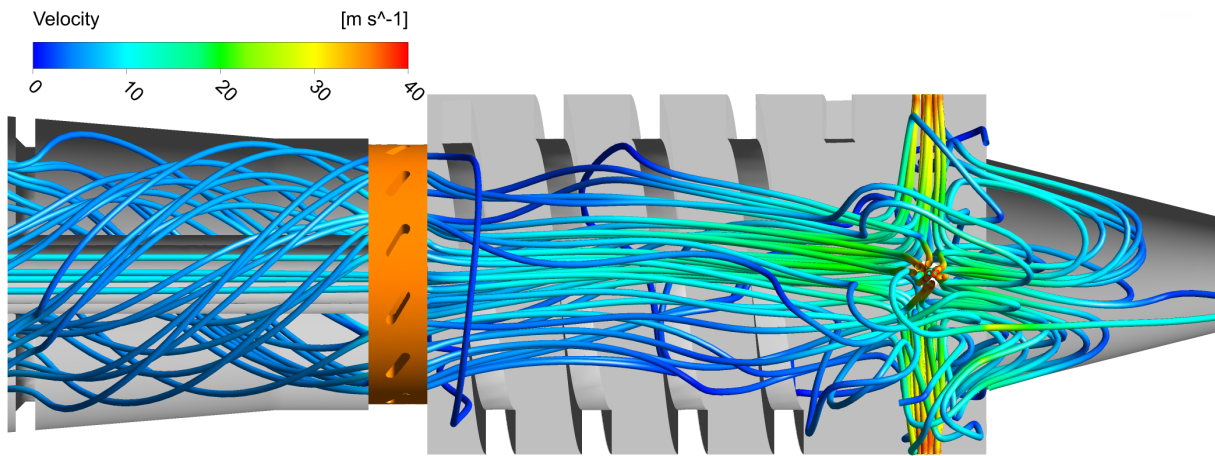


**Figure 7:** Stream lines of the cooling air flow inside the combustion chamber for setup A. The swirl is only generated by the swirlers (orange).

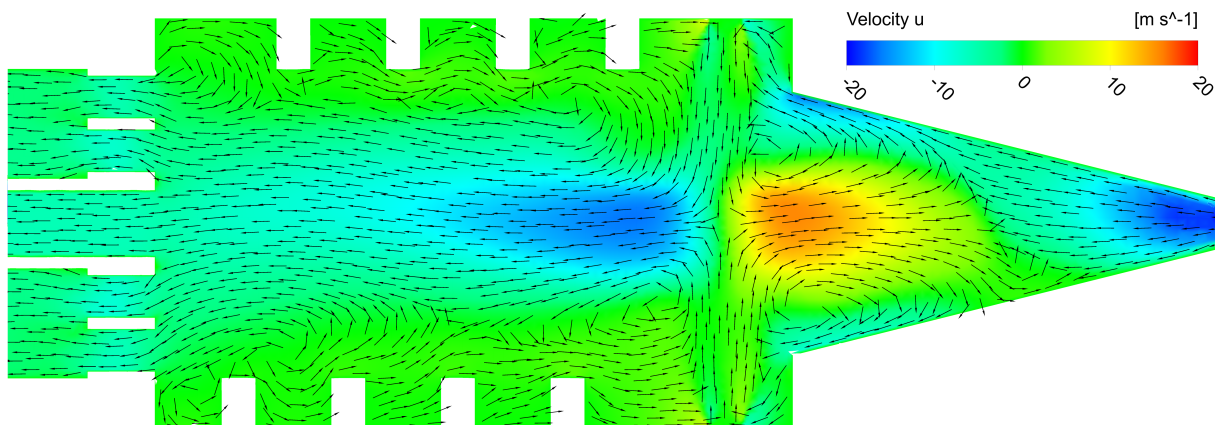


**Figure 8:** Fluid flow inside the combustion chamber for setup B. The colors show the velocity in axial direction. A strong back flow arises at the end of the diffuser. Also, recirculation zones are formed at the spiral's edges.

### 5.3 FLOW THROUGH THE PIPE

The flow through the pipe is illustrated below.

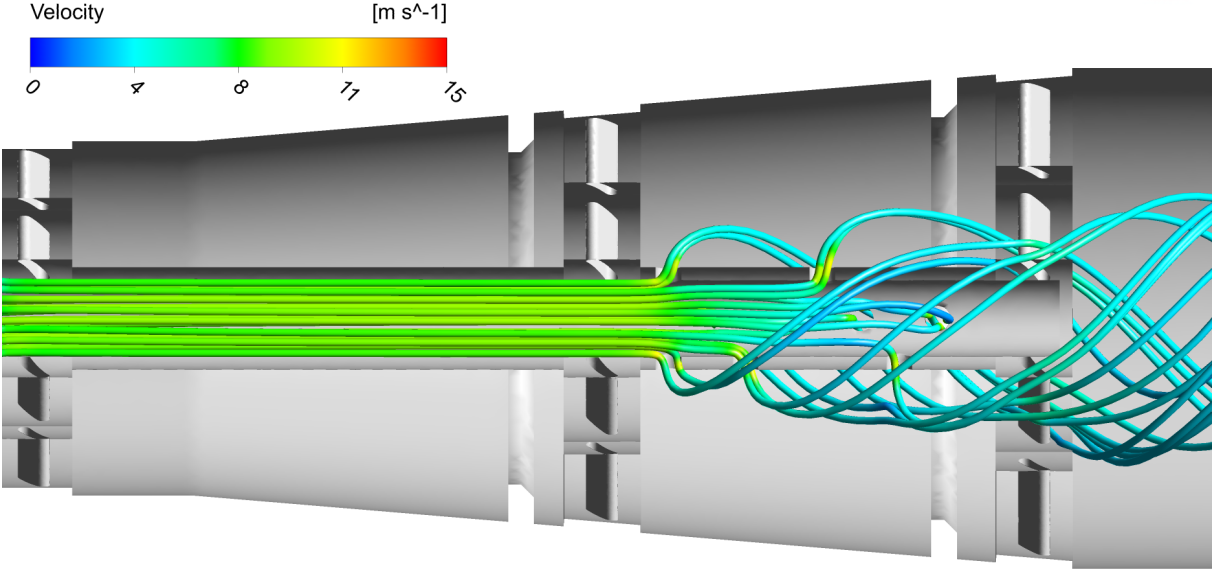


**Figure 9:** Stream lines of the fluid flow through the pipe for setup B.

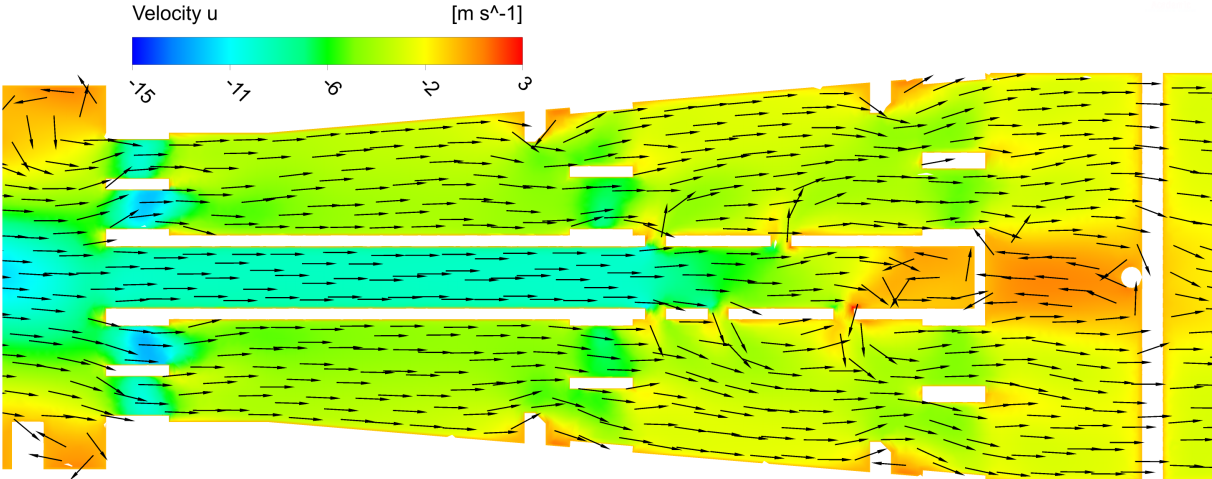


**Figure 10:** Cutting plane illustrating the flow inside the pipe for setup B. The background colors show the velocity in axial direction.

## 5.4 SETUP A ( $\Phi \approx 3.4$ )

In this setup, a fuel rich mixture ( $\Phi \approx 3.4$ ) enters the burner through the nozzles (Figure 2). The air flow rate is set to 0.007 kg/s (Mach  $\approx 0.65$  at the air nozzle outlet). The thermal output based on the fuel flow rate is 70 kW. Because the fuel flow rate is limited by the injector's diameter, the thermal output is quite low compared to the burner's dimensions, and the flame stabilizes at the diffuser entry. Also, the flame burns at the diffuser walls leading to very high wall temperatures. This is discussed later on in section 6.

**Table 1:** Mass flows entering the burner for setup A.

	$T$ [K]	Composition	Mass Flow Rate [kg/s]	
Air Nozzle	300	$Y_{O_2} = 0.233$ , $Y_{N_2} = 0.767$	0.007 ( $\hat{=}$ Mach 0.65)	} $\Phi=3.4$ } $\Phi=0.28$
Fuel Nozzle	300	$Y_{CH_4} = 1$	0.0014	
Cooling Air	300	$Y_{O_2} = 0.233$ , $Y_{N_2} = 0.767$	0.08	

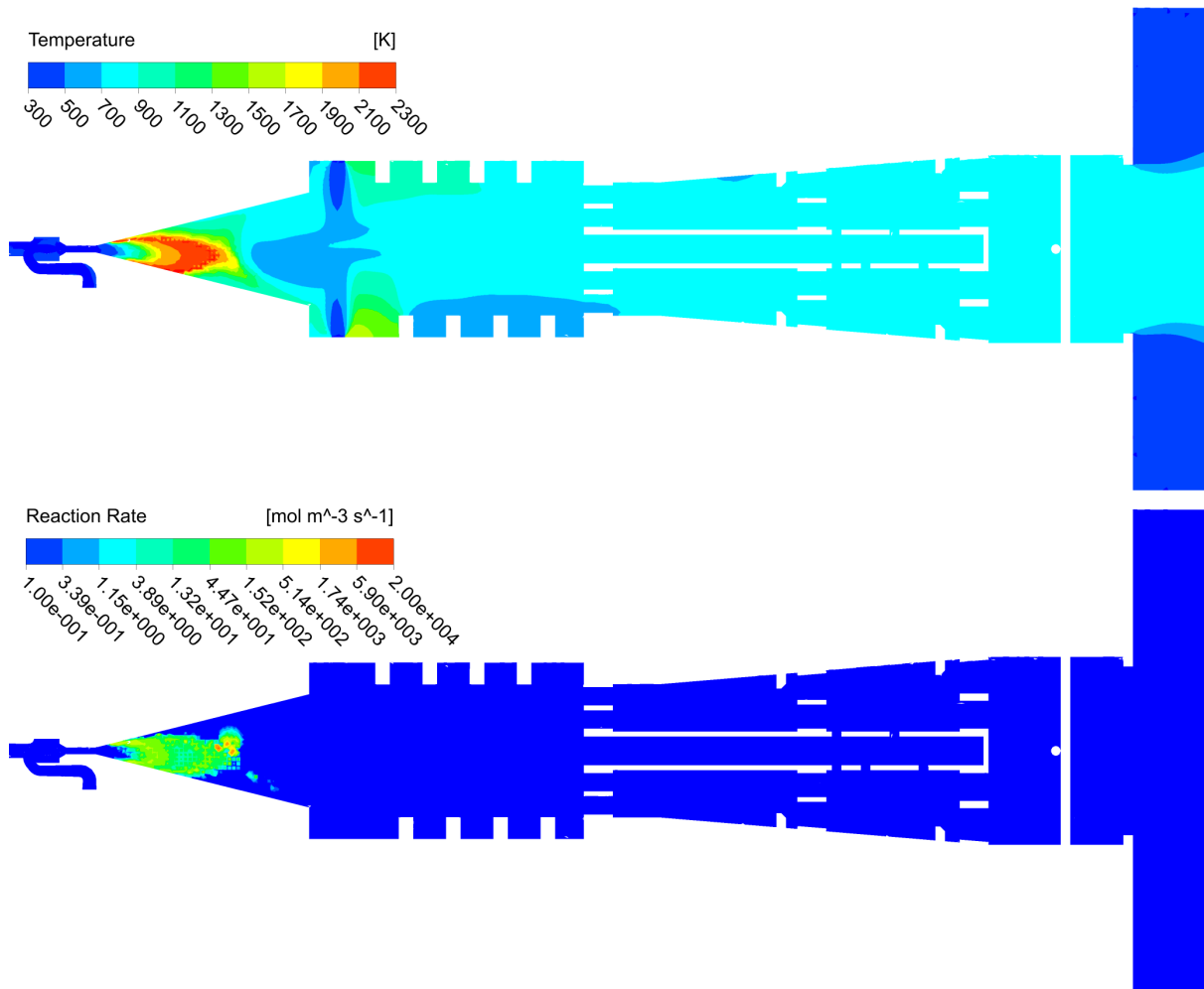


**Figure 11:** Cutting planes showing the temperatures and reaction rates for setup A.

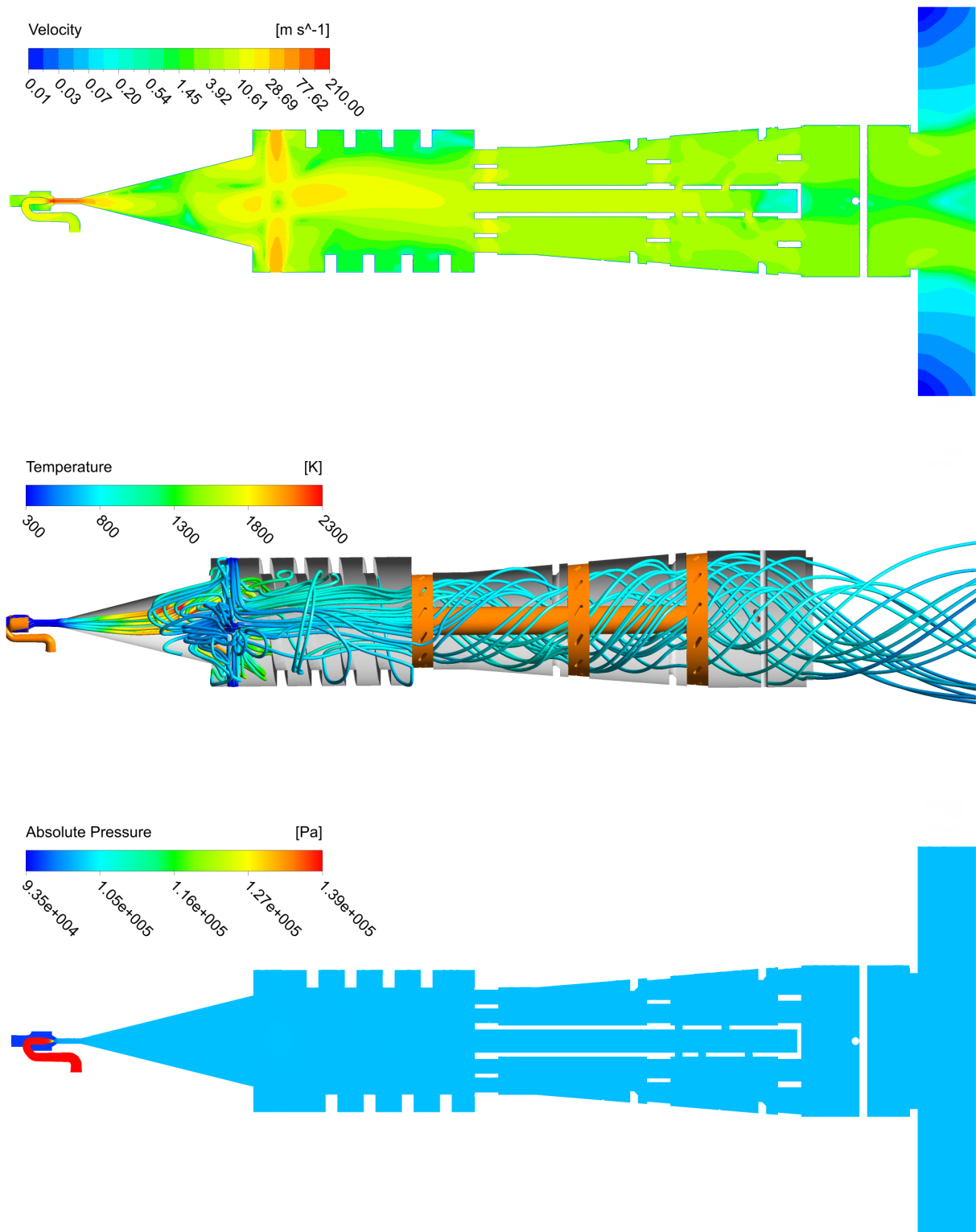


**Figure 12:** Velocities, stream lines colored by temperature, and pressures for setup A.

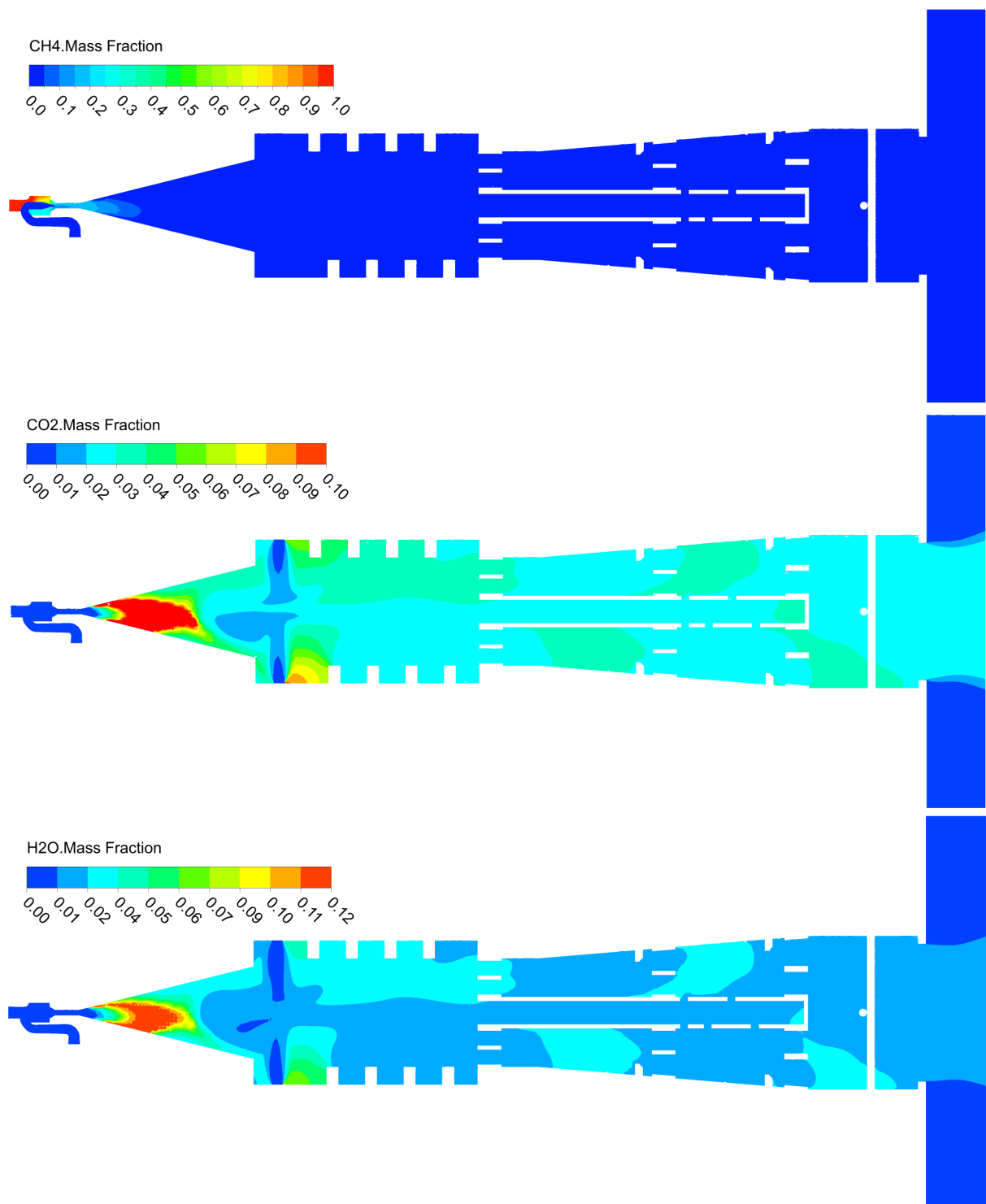


**Figure 13:** *Cutting planes showing the mass fractions for setup A.*

## 5.5 SETUP B ( $\Phi = 1$ )

The air to fuel ratio in this setup is stoichiometric. Because the fuel flow rate is small compared to the cooling air flow rate, the burnt gas is cooled down to about 490 K. The thermal output is 20 kW. As seen in the previous setup, the flame stabilizes at the diffuser entry and burns near the diffuser walls. Due to the unsymmetrical flow pattern inside the injector the flame itself becomes asymmetrical. See section 6 for further discussions.

**Table 2:** Mass flows entering the burner for setup B.

	$T$ [K]	Composition	Mass Flow Rate [kg/s]	
Air Nozzle	300	$Y_{O_2} = 0.233, Y_{N_2} = 0.767$	0.007 ( $\hat{=} \text{Mach } 0.65$ )	} $\Phi=1$ } $\Phi=0.08$
Fuel Nozzle	300	$Y_{CH_4} = 1$	0.000407	
Cooling Air	300	$Y_{O_2} = 0.233, Y_{N_2} = 0.767$	0.08	

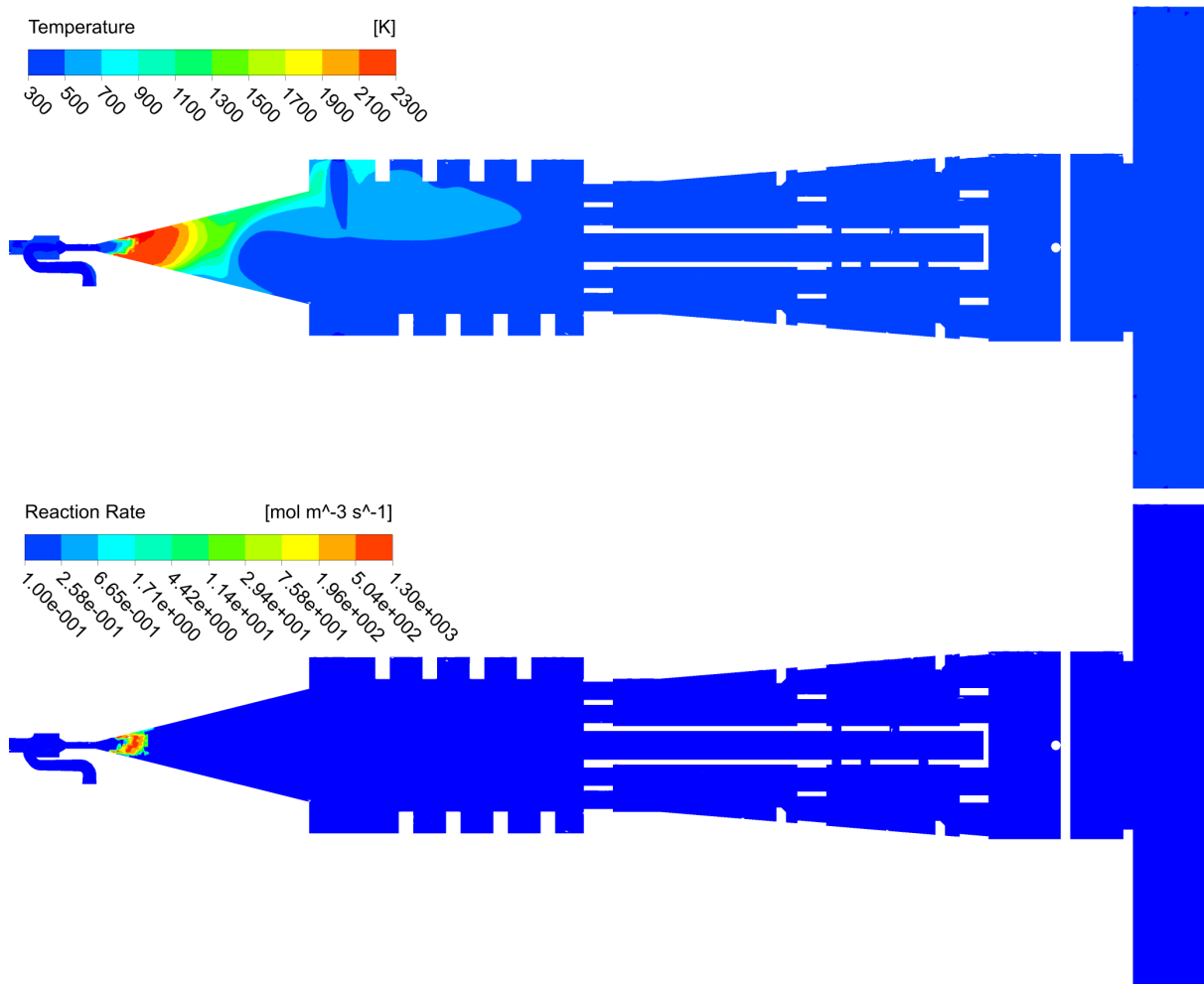


**Figure 14:** Cutting planes showing the temperatures and reaction rates for setup B.

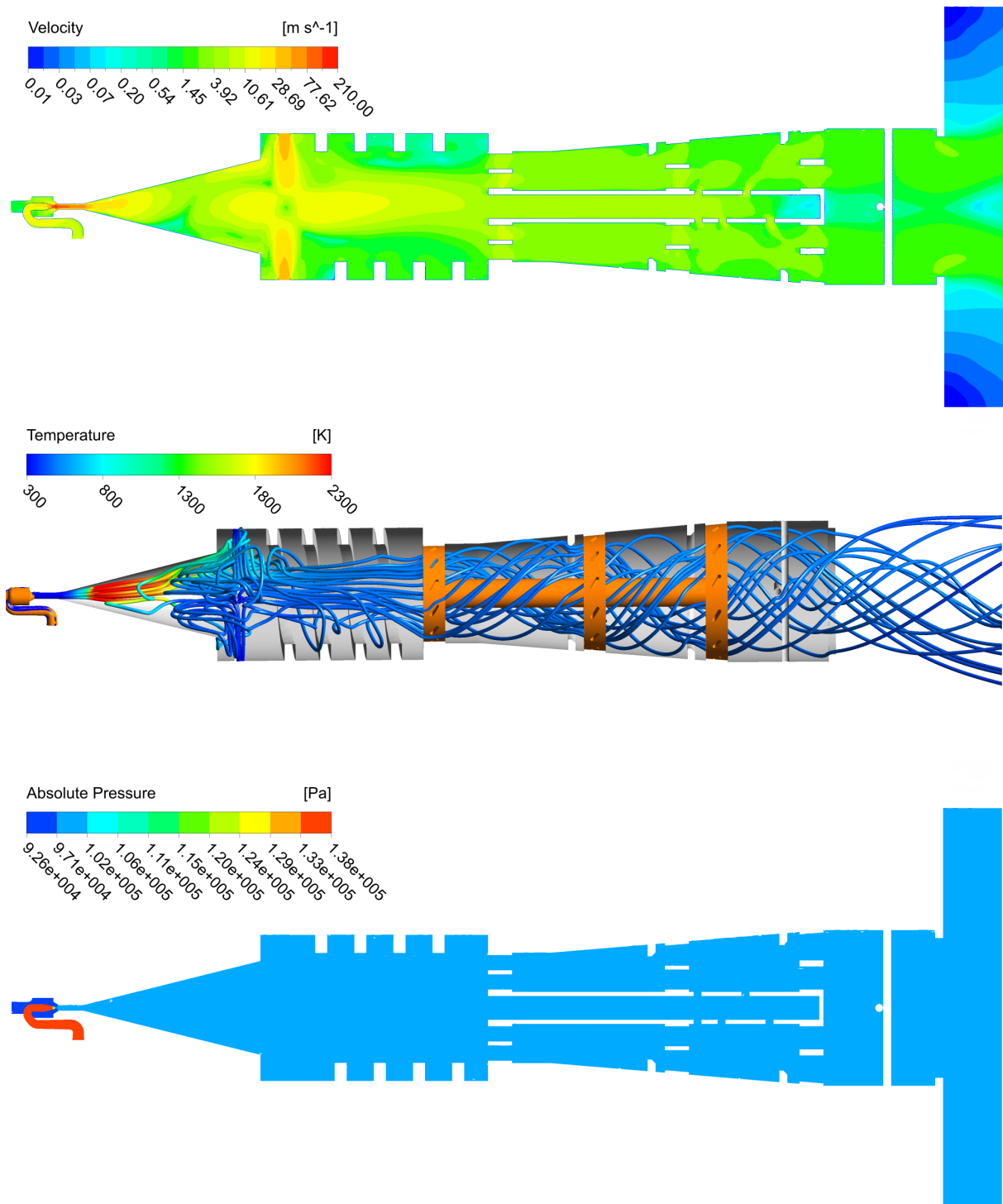


**Figure 15:** Velocities, stream lines colored by temperature, and pressures for setup B.

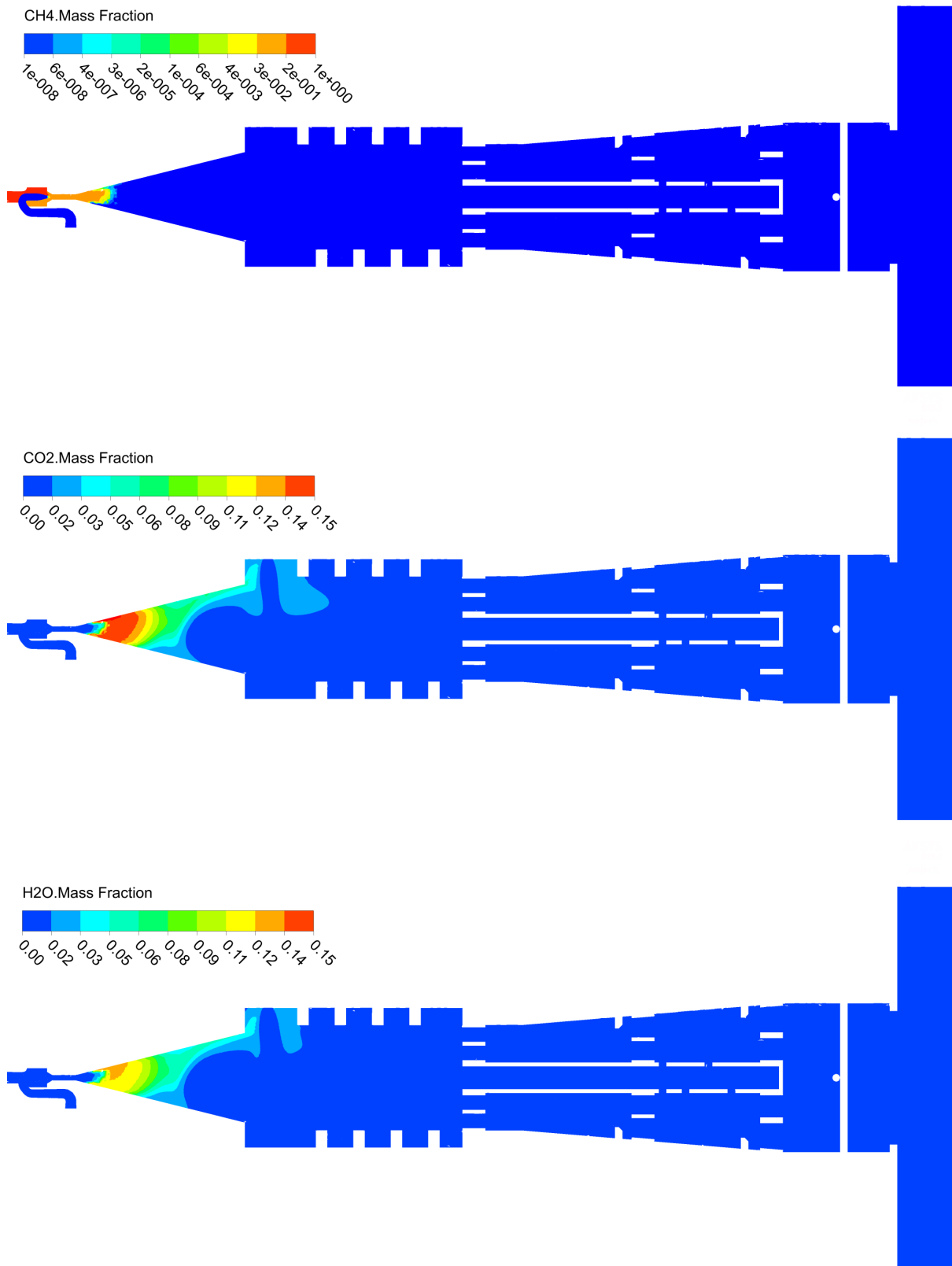


Figure 16: Cutting planes showing the mass fractions for setup B.

## 5.6 SETUP C ( $\Phi \approx 0.83$ )

Setup C is similar to setup B, but a lean mixture is injected, and the fuel flow rate, as well as the air flow rate are higher. Again, the unsymmetrically shaped flame stabilizes at the diffuser entry as a result of the limited mass flow rates and low thermal output (24 kW).

**Table 3:** Mass flows entering the burner for setup C.

	$T$ [K]	Composition	Mass Flow Rate [kg/s]	
Air Nozzle	300	$Y_{O_2} = 0.233, Y_{N_2} = 0.767$	0.01 ( $\hat{=} \text{Mach } 0.8$ )	} $\Phi=0.83$ } $\Phi=0.09$
Fuel Nozzle	300	$Y_{CH_4} = 1$	0.0004867	
Cooling Air	300	$Y_{O_2} = 0.233, Y_{N_2} = 0.767$	0.08	

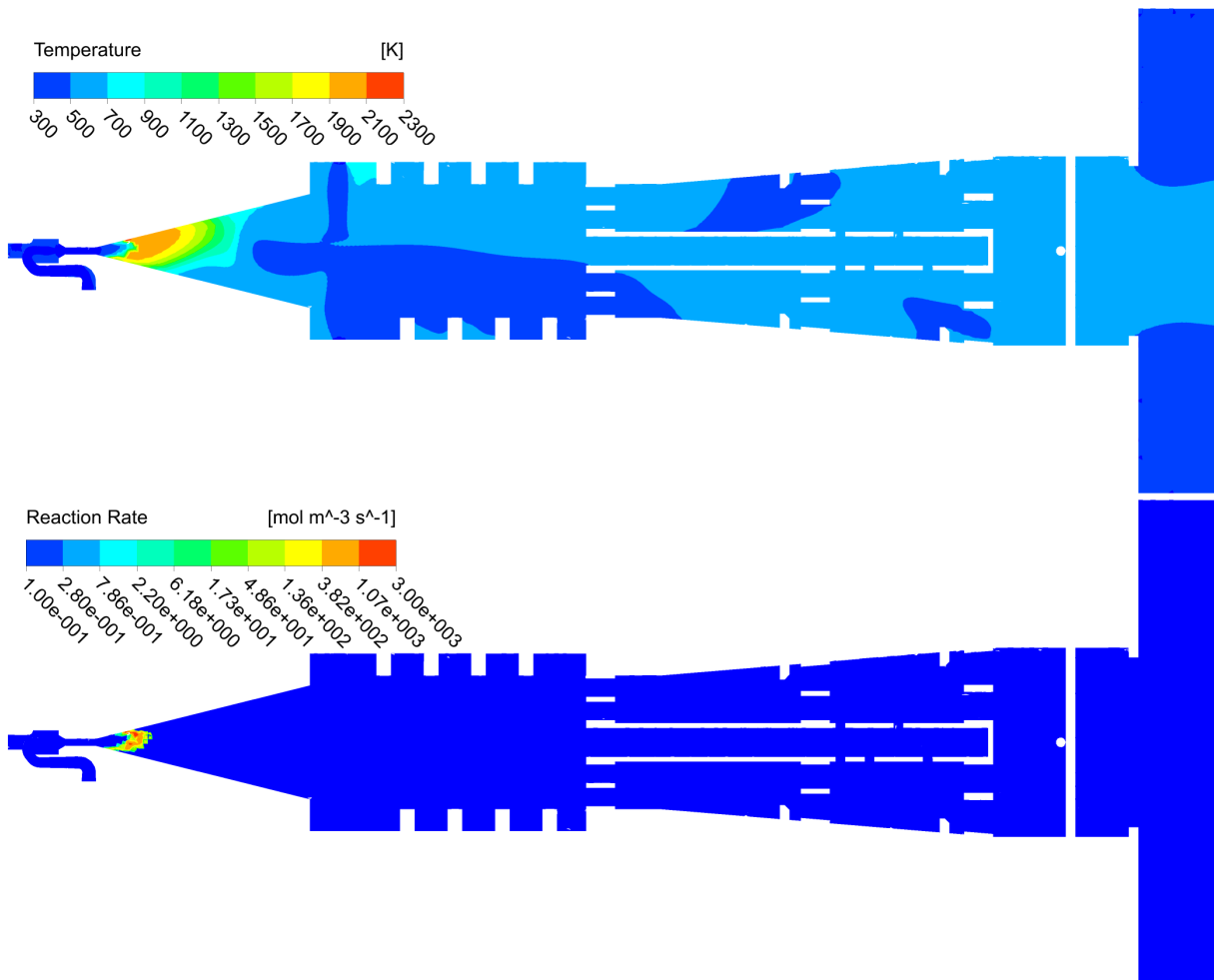


**Figure 17:** Cutting planes showing the temperatures and reaction rates for setup C.

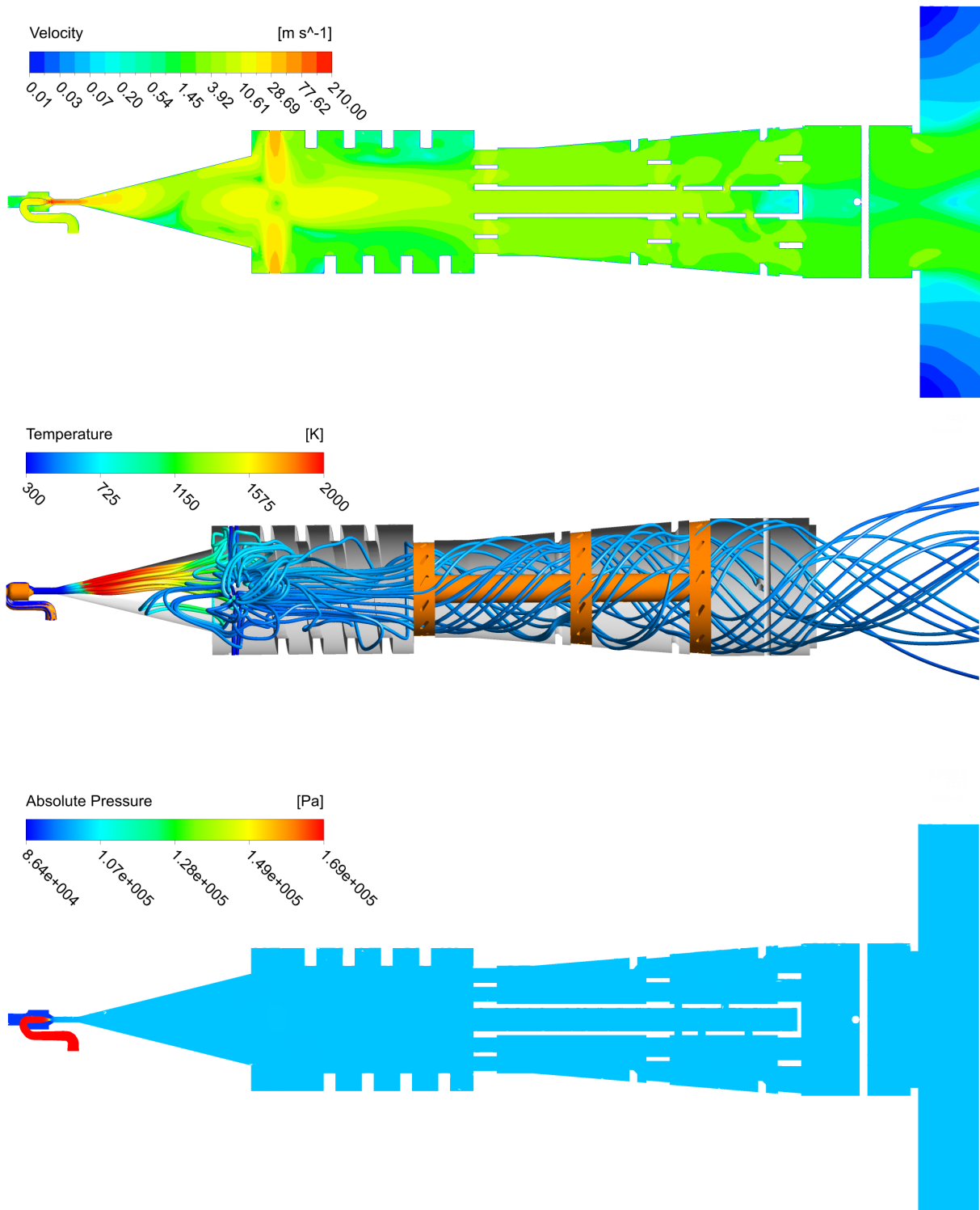


Figure 18: Velocities, stream lines colored by temperature, and pressures for setup C.

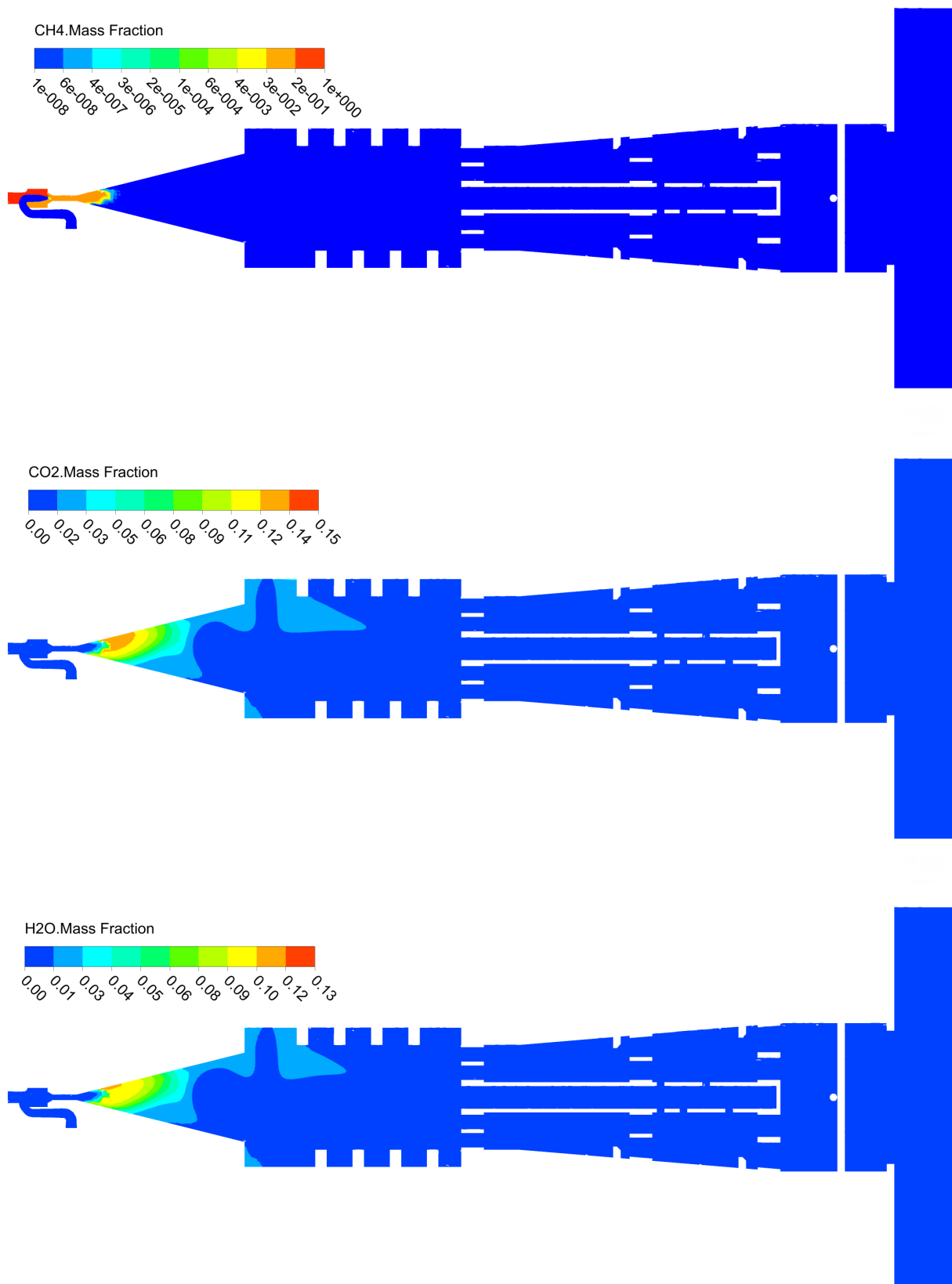


Figure 19: Cutting planes showing the mass fractions for setup C.

## 6 CONCLUSION

Based on the simulation results presented above, three main issues have been identified:

1. As described in subsection 5.2, the spiral inside the combustion chamber does not provide any swirl to the fluid flow. Instead, recirculation zones are formed at the spiral's edges. Therefore, the spiral should be replaced by swirl generators.
2. The air nozzle diameter, as well as the fuel nozzle diameter (see Figure 2), are quite small compared to the burner's dimensions. This limits the air and fuel flow rates, resulting in a low thermal output. The injected air to fuel ratio should be stoichiometric to avoid soot formation. The flame can then be cooled down by the cooling air inside the combustion chamber. To achieve a sufficient thermal output with a stoichiometric mixture, the injector's diameter has to be increased. By increasing the mass flow rates in this way, the flame can be stabilized further downstream inside the diffusor.
3. The asymmetric flow inside the injector leads to recirculation zones containing an ignitable mixture (see subsection 5.1), as well as an asymmetrically shaped flame. For this reason, a symmetrical arrangement of the air and fuel nozzles should be chosen. The injector based on the ejector-jet pump principle has the additional drawback of high pressure loss. Therefore, other designs should be considered. For example, the primary air/fuel mixture could be surrounded by a secondary air flow that stabilizes the flame, and shields the diffusor wall from hot gases.

Furthermore, no apparent purpose of the pipe (see subsection 5.3) can be determined from the simulations performed so far.

After these issues have been addressed by changes in the burner design, further simulations will be conducted with different fuel types.

## 7 LITERATURE RECOMMENDATIONS

Extensive introductions to numerical combustion modeling can be found in:

- T. Poinsot, D. Veynante, Theoretical and numerical combustion, Edwards, Philadelphia, PA, 2005.
- N. Peters, Turbulent combustion, Cambridge monographs on mechanics, Cambridge University Press, Cambridge, 2000.

The CFX 5 program documentation can be found under the name:

ANSYS CFX-Solver Theory Guide 15.0